Theoretical Chemistry Accounts (2018) 137:124
https://doi.org/10.1007/s00214-018-2305-1

REGULAR ARTICLE

QM–MM Ehrenfest dynamics from first principles: photodissociation of diazirine in aqueous solution

Francisco Ramírez[1] · Gonzalo Díaz Mirón[1] · Mariano C. González Lebrero[1] · Damian A. Scherlis[1]

Received: 16 April 2018 / Accepted: 22 August 2018 / Published online: 8 September 2018

Abstract
This article describes an implementation of Ehrenfest molecular dynamics based on TDDFT and Gaussian basis sets, optimized for hybrid QM–MM simulations in GPU. The present method makes use of the equations of motion proposed by Chen et al. (J Chem Phys 135:044126, 2011), which, at variance with previous formulations of the Ehrenfest dynamics, takes into account the movement of the localized basis functions, thus improving accuracy and energy conservation. This methodology is used to explore the evolution and the stability of excited state dynamics for two different constructions of the initial excited state, consisting in the linear response TDDFT S_1 solution, and in the ground state density matrix where the HOMO–LUMO occupancies have been switched, which is a widespread approach to model photoexcitation in electron dynamics simulations. It is found that the second kind of starting state leads to a larger numerical noise and to a poorer stability of the dynamics, aside from "awakening" inner electronic modes that become manifest in the frequency spectrum, and which are absent if the dynamics departs from the linear response TDDFT density matrix. Then, the method is applied to investigate the photodissociation of the diazirine molecule, CH_2N_2, both in vacuum and in aqueous solution. Diazirine decomposes into carbene and molecular nitrogen upon irradiation with UV light, and for this reason it has been widely adopted to photolabel biomolecules through the insertion of carbenes in the macromolecular surface. Our simulations suggest that the quantum yield of the dissociative reaction experiences a decrease in solution with respect to the gas phase, that can be understood in terms of the vibrational relaxation facilitated by the solvent molecules. Besides, the present results indicate that the isomerization and dissociation mechanism occur fully on the S_1 excited state.

Keywords TDDFT · Nonadiabatic dynamics · Photochemistry

1 Introduction

Very often, the fundamental phenomena underlying the behavior of molecules and materials at the nanoscale, including photochemistry, thermally induced excitations, finite-temperature transport, or most electron transfer events, involve nuclear motions beyond a single potential energy surface. The simulation of these processes at a molecular level typically requires the use of nonadiabatic molecular dynamics techniques. Many such schemes have been proposed ever since the formulation of quantum mechanics [1–7]. Among these different approaches, a first distinction can be made between those in which both the electronic and nuclear coordinates are described quantum-mechanically within some approximation [5, 6], and those where the slow degrees of freedom—namely the nuclei—are treated with classical mechanics. Most applications of nonadiabatic dynamics to molecular and extended systems make use of the later kind of methods, usually known as mixed quantum-classical approaches—not to be confused with the hybrid quantum-mechanics molecular-mechanics (QM–MM) methods, which consider part of the interatomic interactions according to a given force field.

Ehrenfest dynamics and surface hopping are the main examples of mixed quantum-classical methodologies [1,

Published as part of the special collection of articles "CHITEL 2017 - Paris - France".

✉ Mariano C. González Lebrero
nanolebrero@qi.fcen.uba.ar

✉ Damian A. Scherlis
damian@qi.fcen.uba.ar

[1] Departamento de Química Inorgánica, Analítica y Química Física, INQUIMAE, Facultad de Ciencias Exactas y Naturales, Universidad de Buenos Aires, Primer Piso Pabellon 2, C1428EHA Ciudad Universitaria, Argentina

3, 7]. In the context of the Ehrenfest method, which is the subject of this work, the time evolution of the coordinates $\mathbf{R}_I$ corresponding to the classical nucleus I is performed self-consistently with that of the electronic wavefunction Ψ according to the following coupled equations:

$$M_I \frac{\partial^2 \mathbf{R}}{\partial t^2}(t) = -\nabla_I \int \Psi^* H_e \Psi \mathrm{d}\mathbf{r} \tag{1}$$

$$i\hbar \frac{\partial \Psi}{\partial t} = H_e \Psi \tag{2}$$

where M_I is the nuclear mass and H_e the electronic Hamiltonian. This pair of equations provides an efficient way to jointly propagate the nuclear and electronic degrees of freedom beyond the Born–Oppenheimer surface. Along the last 20 years several first-principles implementations of the Ehrenfest approach, most of them based on density functional theory (DFT) but also on Hartree–Fock and on multiconfigurational schemes, have been devised and applied with relative success [8–15]. It has to be noticed, however, that the forces on the nuclei given by Eq. (1) rely on the mean-field potential $\langle \Psi | H_e | \Psi \rangle$. When the system approaches a potential energy surface (PES) crossing, or even a region where two hypersurfaces become close in energy, the electronic wavefunction will reflect a mixed quantum population and as a consequence the nuclear forces arising from Eq. (1) will not correspond to a particular PES but to an average. This issue becomes severe in particular when the two—or more—PES rapidly diverge from each other, leading to unphysical trajectories that do not correspond to a well-defined quantum state. The virtues and limitations of the Ehrenfest scheme are well documented in literature [2–4]. Despite its weaknesses, however, Ehrenfest dynamics in combination with first-principles Hamiltonians has proved adequate to model a number of nonadiabatic phenomena, including Coulomb explosion [11], photodissociation of small molecules [16, 17], atomic/molecular collisions [10, 18], radiation damage of biomolecules [18, 19], the photoinduced electron transfer at a semiconductor interface [20], or the photoisomerization of organic molecules [21].

In this article, we present an implementation of Ehrenfest dynamics based on real-time time-dependent density functional theory (RT-TDDFT) and Gaussian basis sets, with the capability to perform hybrid QM–MM calculations [22–24]. This code is efficiently parallelized for graphics processing units (GPU), being able to handle several tens of QM atoms and thousands of MM atoms in electron dynamics simulations with frozen nuclei. By combining molecular dynamics simulations (for configurational sampling) with electron density propagation for an ensemble of geometries, it has been recently applied to spectroscopic investigations in solution and in proteins [23, 25], and to study the molecular conductance of polyacetylene [26]. Here, we focus on the diazirine molecule, CH_2N_2, which is customarily employed as photolabeling agent to identify accessible regions or exposed surfaces in biomolecules, and in particular to characterize protein–protein or protein–ligand interactions [27–29]. As shown in Scheme 1, upon irradiation with near-UV light diazirines decompose into N_2 and carbenes, $:CH_2$, which rapidly and locally insert into C–H, O–H, and N–H bonds. The photochemical mechanism behind this reaction has been a matter of debate for years [16, 30]. In the present contribution, we adopt this system as a case study to examine (a) the incidence that the procedure to construct the initial electronic state has on the Ehrenfest dynamics and (b) the role of the solvent on the photodissociation process. The first issue gains relevance in excited state quantum dynamics simulations, which require the preparation of a proper initial state to propagate the density. A usual practice is to alter the populations by promoting an electron from the HOMO to the LUMO. This choice, which impact has been somehow overlooked in the literature, is confronted here with the more formal approach involving the explicit calculation of the excited wavefunction. Next, we explore the dissociation of the photoexcited diazirine molecule both in vacuum and in solution. To the best of our knowledge, this one is the first TDDFT implementation of Ehrenfest dynamics in a QM–MM framework.

2 Methodology

The Ehrenfest scheme presented here has been implemented as part of the LIO project developed in our group [22–24, 31]. This is an all-electron DFT and RT-TDDFT code with Gaussian basis sets, which employs radial grids to compute the exchange-correlation energy, and in which the most expensive parts of the calculation, including the time propagation of the density matrix, have been ported to CUDA to run in GPU. LIO has been interfaced with the Amber package [32], to perform hybrid quantum-mechanics molecular-mechanics simulations. The total energy is computed according to the electrostatic embedding and the additive formulation:

$$E_{\mathrm{tot}} = E_{\mathrm{QM}} + E_{\mathrm{MM}} + E_{\mathrm{QM\text{-}MM}} \tag{3}$$

where the first term on the right hand side corresponds in this case to the Kohn–Sham energy, the second one to the MM force field potential, and the third one denotes the coupling energy between the classical and quantum regions:

$$E_{\mathrm{QM\text{-}MM}} = \sum_A q_A \int \frac{\rho(\mathbf{r})}{\mathbf{r} - \mathbf{R_A}} \mathrm{d}\mathbf{r} + \sum_{A,B} \frac{q_A Z_B}{\mathbf{R_A} - \mathbf{R_B}} + E^{\mathrm{LJ}}_{\mathrm{QM\text{-}MM}} \tag{4}$$

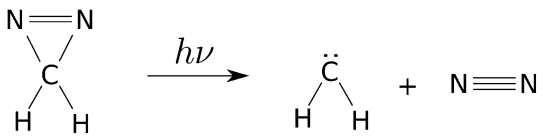

Scheme 1 Decomposition of diazirine into carbene and N_2

Here, $\rho(\mathbf{r})$ is the electron density, q represents the point charges of the MM atoms, Z the nuclear charges of the QM atoms, and $\mathbf{R}$ the nuclear coordinates, with the indices A and B running over the atoms of the classical and the quantum regions, respectively. $E^{\mathrm{LJ}}_{\mathrm{QM\text{-}MM}}$ is a non-electrostatic term, which describes dispersion and short range repulsion effects between QM and MM atoms, using Lennard–Jones potentials, consistently with the MM force field.

For fixed nuclei, the evolution of the wavefunction, Eq. (2), is performed in terms of the density matrix P according to the Liouville–von Neumann equation:

$$i\hbar\frac{\partial P}{\partial t} = [H_{\mathrm{e}}, P] \tag{5}$$

where H_{e} is the matrix associated with the electronic Hamiltonian, and P is expressed in the orthogonal basis of the molecular orbitals. In the LIO code, two routes are available to integrate Eq. (5): the Magnus propagator [33–35], and the much simpler Verlet algorithm to first order. According the later scheme, the electron density at time $t + \Delta t$ is computed by this simple formula:

$$P(t+\Delta t) = \frac{2}{i\hbar}[H_{\mathrm{e}}(t), P(t)]\Delta t + P(t-\Delta t) \tag{6}$$

In this study, we adopted the Verlet propagator because, given its simplicity and its higher sensitivity to the time-step, it offers a more suitable test bed to examine the stability of the dynamics. For further details regarding the real-time TDDFT implementation, we refer the reader to reference [23].

To couple the evolution of the electron and nuclear degrees of freedom in the framework of the Ehrenfest approach, we adopted the formulation by Chen et al. [14]. These authors consider the time-dependence of the basis functions due to the atom dynamics, which gives rise to additional terms in both the electronic and the nuclear equations of motion. Starting from the mixed quantum-classical Lagrangian for electrons and nuclei, the following equations can be derived [14]:

$$i\hbar\frac{\partial P}{\partial t} = [H_{\mathrm{e}} + iD, P] \tag{7}$$

$$\begin{aligned} m_A\frac{\partial^2\mathbf{R_A}}{\partial t^2} = &-\frac{\partial U_{\mathrm{N}}}{\partial\mathbf{R_A}} - Tr\left(\frac{\partial h}{\partial\mathbf{R_A}} + \frac{1}{2}\frac{\partial G}{\partial\mathbf{R_A}}\right) - \frac{\partial E_{xc}}{\partial\mathbf{R_A}} \\ &+ \mathrm{Tr}(S^{-1}\overline{H}_{\mathrm{e}}\overline{P}B_A^{\dagger} + \overline{P}\,\overline{H}_{\mathrm{e}}S^{-1}B_A) \\ &+ iTr(\overline{P}B^{\dagger}S^{-1}B_A + \overline{P}B_A^{\dagger}S^{-1}B) \\ &+ iTr(\overline{P}C_A^{\dagger} - PC_A) \end{aligned} \tag{8}$$

where the first three terms on the right hand side of Eq. (8) are the standard contributions to the nuclear forces in the Born–Oppenheimer approximation. G and S are the Coulomb and overlap matrices, U_{N} the nuclear repulsion, E_{xc} the DFT exchange-correlation energy, m_A the atomic mass, and h stands for the one-electron contributions to the Kohn–Sham Hamiltonian. The upper bars on $\overline{P}$ and $\overline{H}_{\mathrm{e}}$ indicate that these matrices are expressed in the basis of atomic orbitals. B_A is formed with the derivative of the overlap matrix with respect to the position of atom A, while the matrices B, C_A and D depend on this derivative and on the atomic velocities $\mathbf{v_A}$ thus considering the movement of the basis during the propagation.

$$\begin{aligned} [B_A]_{i,j} &= \left\langle \phi_i \middle| \frac{\partial\phi_j}{\partial\mathbf{R_A}} \right\rangle, \quad [B]_{i,j} = \sum_A \left\langle \phi_i \middle| \frac{\partial\phi_j}{\partial\mathbf{R_A}} \right\rangle \cdot \mathbf{v_A} \\ [C_A]_{i,j} &= \sum_B \left\langle \frac{\partial\phi_i}{\partial\mathbf{R_B}} \middle| \frac{\partial\phi_j}{\partial\mathbf{R_A}} \right\rangle \cdot \mathbf{v_B} \end{aligned} \tag{9}$$

$$[D]_{i,j} = \begin{cases} [(-1)(S^{-1/2})^{\dagger}B(S^{-1/2})]_{i,j} & \text{if } i > j \\ [-D]_{j,i} & \text{if } i < j \end{cases} \tag{10}$$

In particular, the formula for the D matrix is valid for $S^{1/2}$ obtained via Cholesky's decomposition of the overlap matrix. The electronic and the nuclear degrees of freedom are evolved simultaneously according to Eqs. (7) and (8), which in the present implementation are integrated with the Verlet algorithm using a common time-step.

The excited density matrices, used as the starting states to propagate the quantum dynamics, were obtained from linear response time-dependent density functional theory (LR-TDDFT) calculations with the program Gaussian09 [36], and properly adapted to be read by the LIO code.

All the simulations reported in this study were performed using the Perdew–Burke–Ernzerhof (PBE) generalized gradient approximation functional [37, 38], employing the 6-31G basis set [39]. This combination of basis and functional seems to be appropriate to provide TDDFT converged results, as suggested by the exploratory calculations which results are summarized in Table 1. This table shows that the description of the excited state and the structural parameters of this molecule are only marginally affected by the choice of basis set or exchange-correlation functional. Unless otherwise noted, the integration time-step (Δt) was 0.0005 fs. In the QM–MM simulations, water molecules were modeled using the TIP3P force field.

Table 1 HOMO–LUMO transition energies, weight of the 11 → 12 excitation, and C–N bond length, computed for the diazirine molecule with LR-TDDFT using the PBE and B3LYP exchange-correlation functionals and different basis sets

XC-functional	Basis set	11 → 12 weight	Transition energy (eV)	C–N distance (Å)
PBE	6-31G	0.70716	3.8250	1.609
	DZVP	0.70693	3.8784	1.558
	TZVP	0.70713	3.8547	1.559
	6-31+G**	0.70709	3.8343	1.557
B3LYP	6-31G	0.70750	3.9152	1.591
	DZVP	0.70743	3.7030	1.548
	TZVP	0.70741	3.8363	1.545
	6-31+G**	0.70714	3.8223	1.545

3 Results and discussion

3.1 The role of the initial state: electron promotion versus LR-TDDFT

Quantum dynamics simulations in excited states entail the construction of a proper starting electronic wavefunction or density matrix. It is a usual practice, in particular in those simulations directly propagating the molecular orbitals, to employ for this purpose the ground state SCF solution in which the HOMO and LUMO populations have been manually exchanged. Hereafter, we will call this kind of construction "electron promotion." While the resulting matrix is not an eigenfunction of the Hamiltonian, it is however normally assumed to be a reasonable representation of the first excited state [16, 40, 41].

The diazirine cyclic bond is experimentally photolyzed using UV light of ~ 310–320 nm. This wavelength is in good agreement with the 85.3 kcal/mol energy obtained with LR-TDDFT for the transition to the first excited singlet S_1, corresponding to 335 nm; this excited state was employed as the initial point to propagate the Ehrenfest dynamics. Figure 1 depicts for the diazirine molecule a pictorial representation of the density matrices corresponding to electron promotion and to the LR-TDDFT excited state, on the left and central panels, respectively. The structure of the later resembles closely the one of the former, aside from a few nonzero off-diagonal elements of almost negligible magnitude, as can be seen on the right panel. This seemingly subtle difference, however, is responsible for notorious discrepancies in the dynamics. The upper panel in Fig. 2 presents the total energy as a function of time for Ehrenfest simulations of the diazirine molecule initiated from the two different density matrices. The one started from the promoted electron state (red curve) shows growing oscillations after the first 300 fs of dynamics and breaks down before reaching the total simulation time. The breaking point can be retarded by using a smaller time-step (green curve). Here, it is important to recognize two different features that are manifest in the trajectories. On the one hand, the energy fluctuations are produced whenever the simulation departs from the electron promotion state, regardless of the time-step. These middle-frequency oscillations in the energy are in principle not related to numerical instabilities, but are inherent

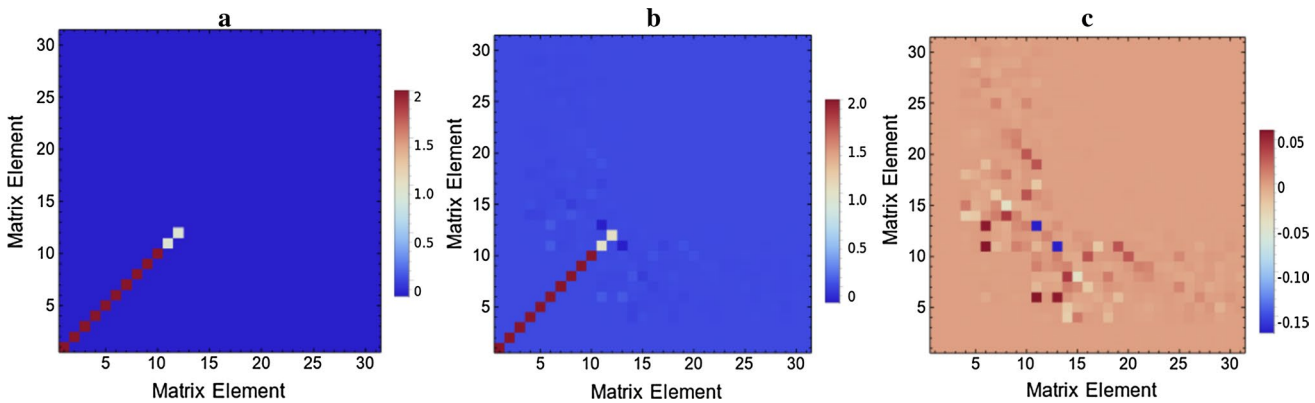

Fig. 1 Graphical representation of the density matrix at time zero, constructed via electron promotion of the SCF solution (**a**), and from a linear response TDDFT calculation (**b**). The right panel shows the difference matrix between (**a**) and (**b**)

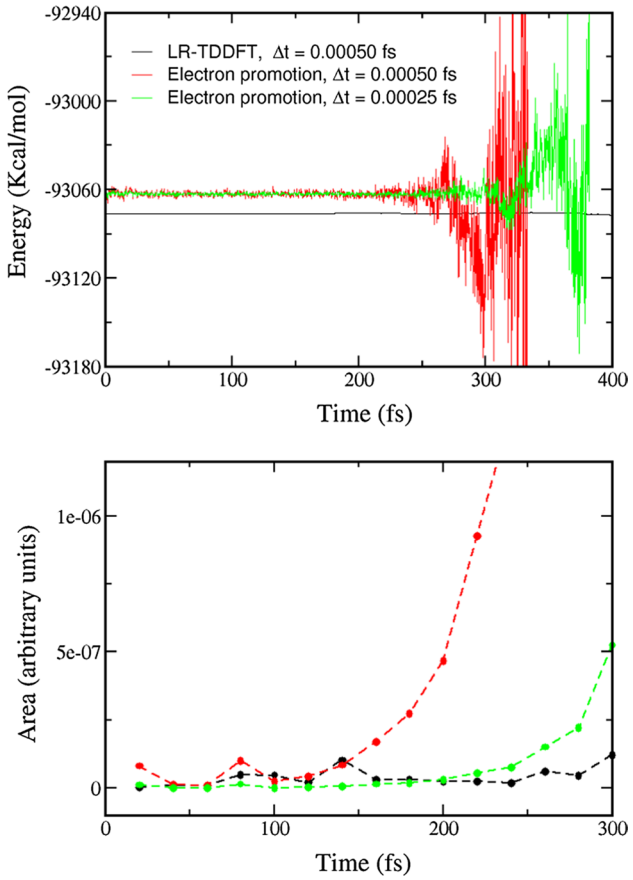

Fig. 2 Top panel: total energy as a function of time, for Ehrenfest simulations started from LR-TDDFT and electron promotion density matrices. In the later case, curves obtained with two different time-steps are shown. Bottom panel: area underneath the peaks associated with high-frequency noise (see text), for the three different dynamics depicted above. The color code is the same as in the top panel

to the initial P and reflect the excitation of modes involving inner electrons, which is a consequence of starting the propagation from an impure state. These excitations or transitions can be identified in a spectral analysis based on the Fourier transform of the dipole moment (data not shown). In other words, the electron promotion construction introduces some degree of "undesired" excitation in the density matrix that develops and becomes manifest in the spectrum.

The second feature is the numerical noise, associated with very high-frequency oscillations that appear at the far end of the spectrum. It is this noise that is responsible for the instability of the numerical integration, because it has a frequency in the order of Δt^{-1}. A possible way to characterize and visualize the magnitude of this noise as a function of time is by the height or the integral of the peaks arising in a frequency spectrum from these fast oscillations. To this end, the trajectory can be split in several consecutive sections—in the present case 15 stretches of 20 fs each, and the Fourier transform of the dipole moment time-correlation function may be computed for each one of these sections. The lower panel of Fig. 2 displays the integral of the high-frequency peaks obtained by Fourier transforming these sections of 20 fs throughout the dynamics. It shows that the use of the TDDFT density matrix as the starting point produces more stable dynamics for the same Δt. Instead, the noise increases progressively when the initial P does not correspond to the legitimate excited state, eventually leading to the divergence of the energy. It can be noticed on the bottom panel of Fig. 2 that at the beginning the noise appears to be less significant for the trajectory initiated from the electron promotion density matrix with $\Delta t = 0.00025$ fs. The smoothness of the propagation naturally depends on the integration step. In spite of this, the LR-TDDFT density matrix (black curve) leads to a more stable trajectory in the end. This result underscores the importance of starting the quantum dynamics from an appropriately calculated, well-converged excited state corresponding to a solution of the electronic Hamiltonian.

3.2 Photodissociation of the diazirine molecule in vacuum and in water

As mentioned in the Introduction, the photochemistry of the family of diazirine compounds has been examined by several authors throughout the last decades, both experimentally and computationally [16, 30, 42–47], namely motivated for its application in the labeling of accessible surfaces in proteins and biomolecules but also for the importance of carbenes in different organic synthesis routes [27, 30]. A qualitative picture of the S_0 and S_1 state potential energy surfaces is sketched in Fig. 3. The energetic differences between isomers were calculated with DFT and LR-TDDFT minimizations in the ground and excited states, respectively.

A total of 30 different Ehrenfest trajectories of length 400 fs were performed, of which one half were in the gas phase and the other in aqueous solution using the QM–MM approach. Each one of these trajectories were started from a different initial geometry generated from ground state Born–Oppenheimer molecular dynamics simulations thermalyzed at 300 K, either in vacuum or in water. The first excited state S_1 obtained from LR-TDDFT, described in the previous section, was adopted in all cases as the initial density matrix. In this way, a Franck–Condon transition is implicitly assumed to model the photochemical process. The QM–MM simulations were conducted in periodic boundary conditions in a cell of dimensions 24.862 Å × 24.896 Å × 25.219 Å, including 446 water molecules.

With just one exception, the CN_2 cycle of the diazirine—but not necessarily the molecule—is broken within the first 400 fs of dynamics. In Fig. 4, the C–N distance

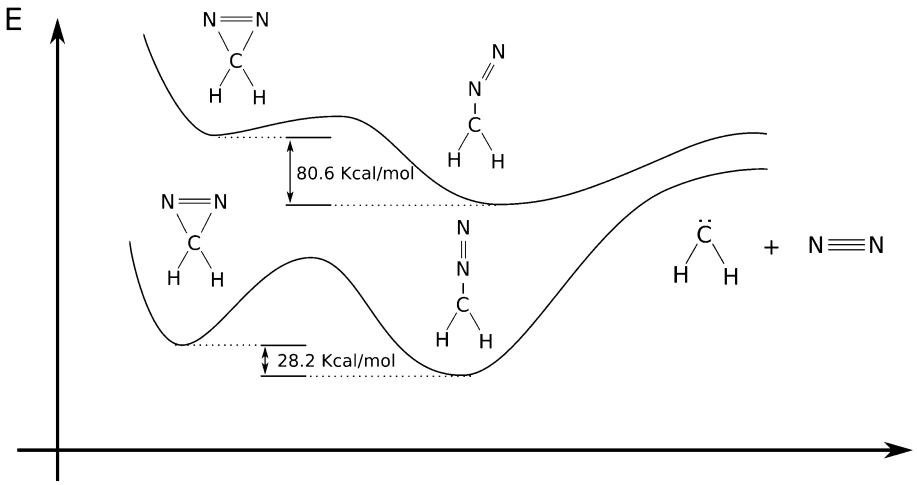

Fig. 3 Sketch of the potential energy surfaces for the ground and first excited singlet states along the dissociation path of the diazirine molecule. The energetic differences correspond to DFT and LR-TDDFT minimizations, respectively

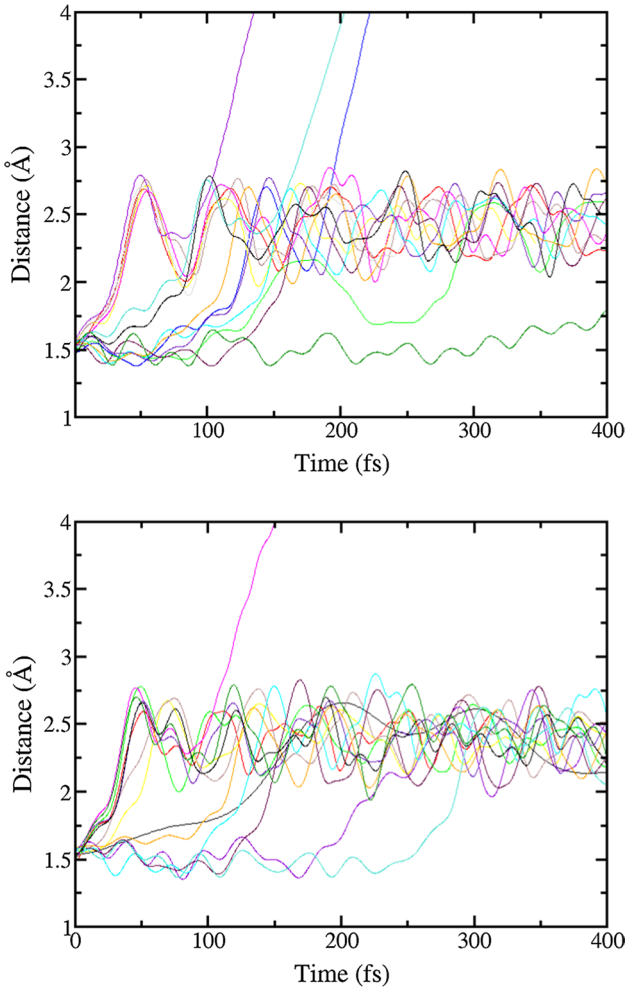

Fig. 4 Depiction of the C–N distance corresponding to the broken bond as a function of time, for Ehrenfest molecular dynamics initiated from the S_1 state of diazirine, in vacuum (top panel) and in solution (bottom panel)

corresponding to the broken bond is plotted as a function of time. The elongation from ~ 1.5 to ~ 2.5 Å points out the isomerization of the diazirine molecule to diazomethane. It can be seen that a small fraction of these trajectories—three in vacuum and only one in the solvent—leads to photodissociation within the length of the simulation. Figure 5 depicts a sequence of structures illustrating the dissociation process in aqueous solution. The first jump in the C–N distance appearing in Fig. 4 corresponds to an isomerization to diazomethane, which exhibits a slightly angular geometry in the excited state. The lifetime of this species has been experimentally established in a few picoseconds, depending on substituents and on the solvent [30, 46, 47]. A further separation of the C and N atoms seen in Fig. 4 marks the initial stages of photodissociation. The small proportion of dissociative trajectories observed in 0.4 ps of dynamics—20% in the gas phase and less than 10% in vacuum—is consistent with the order of the experimental lifetimes.

In principle, the fragmentation appears to be more likely in the gas phase than it is in solution. No conclusive assessment can be made, however, given the relatively small amount of available trajectories. In any case, if there is any solvent effect, it must be through the vibrational quenching of the S_1 state. The low dipole moments of diazirine and diazomethane are hardly affected by hydration, and negligible changes in the atomic Mulliken populations are observed when going from vacuum to solution. So, it seems unlikely that the aqueous environment decreases the photochemical yield via a polarization mechanism. Instead, it has to be noticed that the energy difference between the diazirine and diazomethane isomers is of nearly 80 kcal/mol on the S_1 surface (see Fig. 3). This implies that the isomerization in the excited state must leave a "vibrationally hot" diazomethane, which dissociation is likely to occur. The analysis of the molecular temperature for the diazomethane formed in the Ehrenfest dynamics reveals a mean value of ~ 2500 K, roughly consistent with an energy of 80 kcal/mol distributed

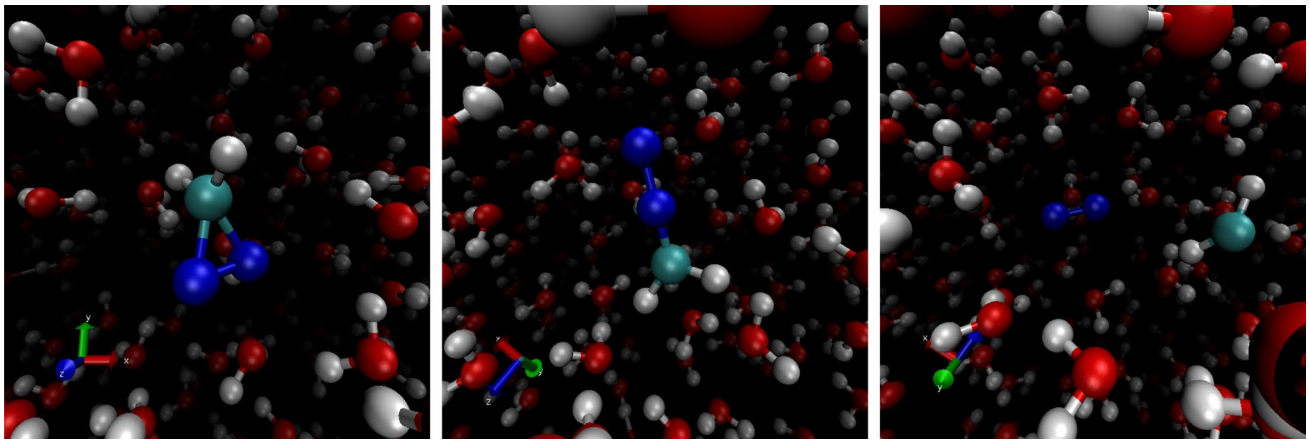

Fig. 5 Sequence of snapshots extracted from Ehrenfest molecular dynamics, illustrating the photodissociation of the diazirine molecule in aqueous solution. Nitrogen, carbon, oxygen, and hydrogen atoms are represented in blue, cyan, red, and white colors, respectively

Table 2 Kinetic, potential, and total energy (kcal/mol) corresponding to the dissociating mode in the excited state at the beginning of each Ehrenfest trajectory in vacuum

Trajectory no.	Kinetic E	Potential E	Total E
1	7.08E−03	1.45E−02	2.15E−02
2	6.34E−02	3.39	3.45
3	0.401	1.85	2.25
4	0.440	5.13	5.57
5	0.300	36.6	36.9
6	5.46E−02	7.23	7.29
7	0.755	5.17	5.93
8	**1.19**	**15.7**	**16.9**
9	0.296	35.9	36.3
10	0.132	47.2	47.3
11	5.31E-02	48.9	48.9
12	**0.112**	**85.9**	**86.0**
13	0.393	44.4	44.8
14	**0.873**	**32.4**	**33.3**
15	0.132	5.50	5.63

The potential energy is given relative to the optimized S_1 state

Those trajectories leading to dissociation are highlighted in bold characters

in the 15 degrees of freedom of CH_2N_2. The solvent can make a difference here through the thermal deactivation of the excited vibrational modes. Table 2 presents the kinetic, potential, and total energies corresponding to the dissociating mode in the S_1 state at the beginning of the different gas phase trajectories. These values have been assigned according to the normal mode coordinates, considering the atomic masses and velocities for the kinetic energy, and the harmonic force constants and equilibrium displacements for the potential contribution. The three cases ending up in dissociation (trajectories # 8, 12, and 14) are highlighted in bold characters. It can be seen that there is no direct correlation between dissociation and the total energy of the corresponding mode. However, the dynamics that do dissociate are those having the highest kinetic energies in that mode, or, in the case of trajectory #8, having a very high potential energy. No correlation is found, on the other hand, between dissociation and the kinetic or potential energies of the full molecule.

The lifetime of the excited diazirine, estimated as the time elapsed until the first maxima above 2.5 Å is reached in Fig. 4, does not seem to be significantly affected by the environment. The average value of 113 fs in vacuum is not statistically different from the mean value in solution, of 118 fs. The variance, however, is larger in the later case: the higher number of configurations accessible in the presence of the solvent can be expected to diversify the reactive pathways. On the other hand, the evolution of the density matrices throughout the dynamics, presented in Fig. 6, reveals that the structure of P is always conserved, implying that dissociation takes place on the S_1 surface, in agreement with the results of Ehrenfest simulations by Lee et al. [16], and in opposition to the static highly correlated quantum chemistry calculations by Olivucci and collaborators postulating a S_1/S_0 conical intersection [44, 48].

4 Summary and final remarks

We have presented in this work an Ehrenfest molecular dynamics implementation based on TDDFT and Gaussian basis sets, devised for hybrid QM–MM simulations. This code is part of the LIO project, a DFT package efficiently optimized for CPU and GPU computing [24]. Using this scheme, we have investigated the impact that the way chosen to construct the departure state has on the quantum

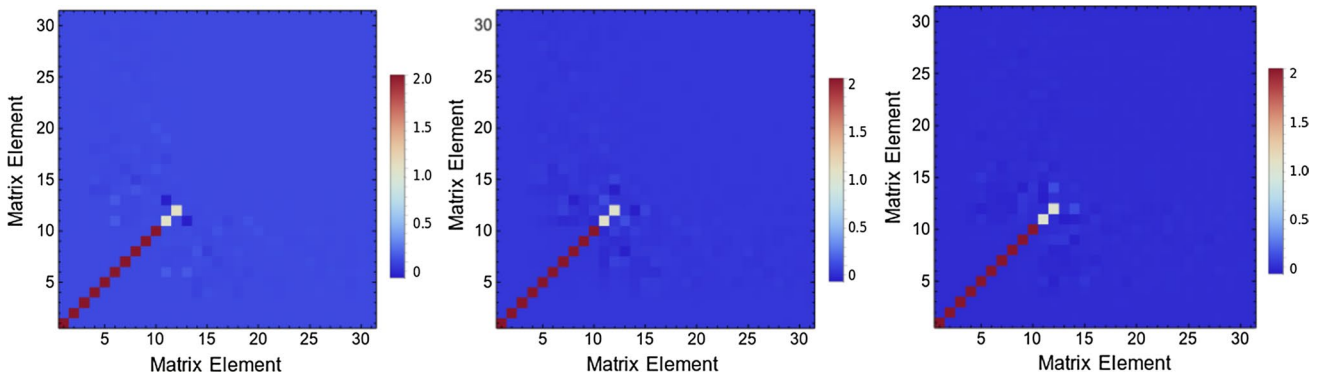

Fig. 6 Graphical representation of the density matrix at various stages of an Ehrenfest dynamics of the dissociation of the diazirine molecule, started from the first singlet excited state. The density matrices shown correspond to the initial state (left), the diazomethane isomer (center), and the dissociated system (right)

dynamics in the excited state. To this end, we compared the performance achieved using either the linear response TDDFT solution, or a configuration obtained by switching the HOMO–LUMO occupations in the ground state density matrix. This second procedure proved to have two undesired consequences: on one hand, it introduces spurious modes in the dynamics, arising from the fact that the starting density matrix does not correspond to a pure state. On the other, it produces numerical instabilities that eventually lead to the divergence of the energy at earlier times in comparison with those dynamics initiated from the LR-TDDFT solution.

The results obtained from the molecular dynamics simulations of diazirine in the excited state suggest that the quantum yield of the photolysis drops in aqueous media, basically due to the thermal deactivation of excited vibrational states. The isomerization of the diazirine molecule to diazomethane in the excited surface is highly exothermic, and therefore the later species is formed energetically activated. Thus, the solvent can partially preclude the path to dissociation through thermal decay. In all the cases investigated in the present simulations, the photochemical decomposition of diazirine proceeded in the S_1 state without any change in the electronic occupations.

This study is, to the best of our knowledge, the first one to report nonadiabatic molecular dynamics from first principles in a QM–MM setting. This methodology opens the door to investigate at the molecular and electronic level, a wealth of phenomena which is very difficult to address with either experimental or theoretical tools. Electron transport at finite temperature across biomolecules or nanostructures, photochemistry in solution, or electron exchange at a solid–liquid interface, are examples of fundamental nonadiabatic processes in complex environments where the scheme introduced in this article can make substantial contributions. By restraining the QM description to a few atoms determining the electron-ion dynamics, and representing the rest of the system with a classical force field, this technique becomes a powerful instrument for out-of-equilibrium simulations with thousands of atoms.

Acknowledgements FR and GDM acknowledge CONICET for doctoral fellowships. This study has been supported by Grants of ANPCYT/PICT 2012-2292 and UBACYT 20020160100124BA.

References

1. Marx D, Hutter J (2009) Ab initio molecular dynamics. Cambridge University Press, Cambridge
2. Hack MD, Truhlar DG (2000) Nonadiabatic trajectories at an exhibition. J Phys Chem A 104:7917
3. Tully JC (2012) Perspective: nonadiabatic dynamics theory. J Chem Phys 137:22A301
4. Persico M, Granucci G (2014) An overview of nonadiabatic dynamics simulations methods, with focus on the direct approach versus the fitting of potential energy surfaces. Theor Chem Acc 133:1526
5. de Carvalho FF, Bouduban MEF, Curchod BFE, Tavernelli I (2014) Nonadiabatic molecular dynamics based on trajectories. Entropy 16:62
6. Curchod BFE, Martínez TJ (2018) Ab initio nonadiabatic quantum molecular dynamics based on trajectories. Chem Rev 18:3305
7. Wang L, Akimov A, Prezhdo OV (2016) Recent progress in surface hopping: 2011–2015. J Phys Chem Lett 7(11):2100
8. Klein S, Bearpark MJ, Smith BR, Robb MA, Olivucci M, Bernardi F (1998) Mixed state 'on the fly' non-adiabatic dynamics: the role of the conical intersection topology. Chem Phys Lett 292:259
9. Stier W, Prezhdo OV (2003) Non-adiabatic molecular dynamics simulation of ultrafast solar cell electron transfer. J Mol Struct Theochem 630:33 (**WATOC '02 Special Issue**)
10. Isborn CM, Li X, Tully JC (2007) Time-dependent density functional theory Ehrenfest dynamics: collisions between atomic oxygen and graphite clusters. J Chem Phys 126:134307
11. Kawashita Y, Nakatsukasa T, Yabana K (2009) Time-dependent density-functional theory simulation for electron–ion dynamics in molecules under intense laser pulses. J Phys Condens Matter 21:064222
12. Li X, Tully JC, Schlegel HB, Frisch MJ (2005) Ab initio Ehrenfest dynamics. J Chem Phys 123:084106

13. Liang W, Chapman CT, Li X (2011) Efficient first-principles electronic dynamics. J Chem Phys 134:184102
14. Wang F, Yam CY, Hu L, Chen G (2011) Time-dependent density functional theory based Ehrenfest dynamics. J Chem Phys 135:044126
15. Miyamoto Y, Rubio A (2018) Application of the real-time time-dependent density functional theory to excited-state dynamics of molecules and 2D materials. J Phys Soc Jpn 87(4):041016
16. Lee H, Miyamoto Y, Tateyama Y (2009) Excited state carbene formation from UV irradiated diazomethane. J Organ Chem 74:562
17. Liang W, Isborn CM, Lindsay A, Li X, Smith SM, Levis RJ (2010) Time-dependent density functional theory calculations of Ehrenfest dynamics of laser controlled dissociation of no+: pulse length and sequential multiple single-photon processes. J Phys Chem A 114:6201
18. Seraide R, Bernal MA, Brunetto G, de Giovannini U, Rubio A (2017) TDDFT-based study on the proton–DNA collision. J Phys Chem B 121:7276
19. Kohanoff J, McAllister M, Tribello GA, Gu B (2017) Interactions between low energy electrons and DNA: a perspective from first-principles simulations. J Phys Condens Matter 29:383001
20. Duncan WR, Stier WM, Prezhdo OV (2005) Ab initio nonadiabatic molecular dynamics of the ultrafast electron injection across the Alizarin−TiO2 interface. J Am Chem Soc 127(21):7941
21. Miyamoto Y, Tateyama Y, Oyama N, Ohno T (2015) Conservation of the pure adiabatic state in Ehrenfest dynamics of the photoisomerization of molecules. Sci Rep 5:18220
22. Nitsche MA, Ferreria M, Mocskos EE, Lebrero MCG (2014) GPU accelerated implementation of density functional theory for hybrid QM/MM simulations. J Chem Theory Comput 10(3):959
23. Morzan UN, Ramírez FF, Oviedo MB, Sánchez CG, Scherlis DA, Lebrero MCG (2014) Electron dynamics in complex environments with real-time time dependent density functional theory in a QM–MM framework. J Chem Phys 140(16):164105
24. The LIO Project. https://github.com/MALBECC/LIO
25. Marcolongo JP, Morzan UN, Zeida A, Scherlis DA, Olabe JA (2016) Nitrosodisulfide [s2no]- (perthionitrite) is a true intermediate during the "cross-talk" of nitrosyl and sulfide. Phys Chem Chem Phys 18:30047
26. Morzan UN, Ramrez FF, Lebrero MCG, Scherlis DA (2017) Electron transport in real time from first-principles. J Chem Phys 146(4):044110
27. Murale DP, Hong SC, Haque MM, Lee JS (2017) Photo-affinity labeling (PAL) in chemical proteomics: a handy tool to investigate protein–protein interactions (PPIS). Proteome Sci 15:14
28. Gómez G, Mundo M, Craig P, Delfino J (2012) Probing protein surface with a solvent mimetic carbene coupled to detection by mass spectrometry. J Am Soc Mass Spectrom 23(1):30
29. Gmez G, Monti J, Mundo M, Delfino J (2015) Solvent mimicry with methylene carbene to probe protein topography. Anal Chem 87(19):10080
30. Platz MS (2014) A perspective on physical organic chemistry. J Organ Chem 79:2341
31. Marcolongo JP, Zeida A, Semelak JA, Foglia NO, Morzan UN, Estrin DA, González Lebrero MC, Scherlis DA (2018) Chemical reactivity and spectroscopy explored from QM/MM molecular dynamics simulations using the lio code. Front Chem 6:70
32. Pearlman D, Case D, Caldwell J, Ross W, Cheatham T, DeBolt S (1995) Amber, a package of computer programs for applying molecular mechanics, normal mode analysis, molecular dynamics and free energy calculations to simulate the structural and energetic properties of molecules. Comput Phys Commun 91:1
33. Magnus W (1954) On the exponential solution of differential equations for a linear operator. Commun Pure Appl Math 7:649
34. Tannor DJ (2007) Introduction to quantum mechanics. A time-dependent perspective. University Science Books, Herndon
35. Castro A, Marques MAL, Rubio A (2004) Propagators for the time-dependent Kohn–Sham equations. J Chem Phys 121(8):3425
36. Frisch MJ, Trucks GW, Schlegel HB, Scuseria GE, Robb MA, Cheeseman JR, Scalmani G, Barone V, Mennucci B, Petersson GA, Nakatsuji H, Caricato M, Li X, Hratchian HP, Izmaylov AF, Bloino J, Zheng G, Sonnenberg JL, Hada M, Ehara M, Toyota K, Fukuda R, Hasegawa J, Ishida M, Nakajima T, Honda Y, Kitao O, Nakai H, Vreven T, Montgomery JA, Jr, Peralta JE, Ogliaro F, Bearpark M, Heyd JJ, Brothers E, Kudin KN, Staroverov VN, Kobayashi R, Normand J, Raghavachari K, Rendell A, Burant JC, Iyengar SS, Tomasi J, Cossi M, Rega N, Millam JM, Klene M, Knox JE, Cross JB, Bakken V, Adamo C, Jaramillo J, Gomperts R, Stratmann RE, Yazyev O, Austin AJ, Cammi R, Pomelli C, Ochterski JW, Martin RL, Morokuma K, Zakrzewski VG, Voth GA, Salvador P, Dannenberg JJ, Dapprich S, Daniels AD, Farkas, Foresman JB, Ortiz JV, Cioslowski J, Fox DJ (2009) Gaussian09 Revision E.01. Gaussian Inc. Wallingford CT
37. Perdew JP, Burke K, Ernzerhof M (1996) Generalized gradient approximation made simple. Phys Rev Lett 77:3865
38. Perdew JP, Burke K, Ernzerhof M (1997) Generalized gradient approximation made simple. Phys Rev Lett 78:1396
39. Hehre WJ, Ditchfield R, Pople JA (1972) Self consistent molecular orbital methods. XII. Further extensions of gaussian-type basis sets for use in molecular orbital studies of organic molecules. J Chem Phys 56(5):2257
40. Tateyama Y, Oyama N, Ohno T, Miyamoto Y (2006) Real-time propagation time-dependent density functional theory study on the ring-opening transformation of the photoexcited crystalline benzene. J Chem Phys 124(12):124507
41. Meng S, Kaxiras E (2008) Real-time, local basis-set implementation of time-dependent density functional theory for excited state dynamics simulations. J Chem Phys 129(5):054110
42. Modarelli DA, Platz MS (1991) Interception of dimethylcarbene with pyridine: a laser flash photolysis study. J Am Chem Soc 113(23):8985
43. Seburg RA, McMahon RJ (1992) Photochemistry of matrix-isolated diazoethane and methyldiazirine: ethylidene trapping? J Am Chem Soc 114(18):7183
44. Yamamoto N, Bernardi F, Bottoni A, Olivucci M, Robb MA, Wilsey S (1994) Mechanism of carbene formation from the excited states of diazirine and diazomethane: an MC-SCF study. J Am Chem Soc 116(5):2064
45. Bonneau R, Liu MT (1996) Quantum yield of formation of diazo compounds from the photolysis of diazirines. J Am Chem Soc 118(30):7229
46. Burdzinski G, Réhault J, Wang J, Platz MS (2008) A study of the photochemistry of diazo Meldrum's acid by ultrafast time-resolved spectroscopies. J Phys Chem A 112(41):10108
47. Zhang Y, Burdzinski G, Kubicki J, Vyas S, Hadad CM, Sliwa M, Poizat O, Buntinx G, Platz MS (2009) Study of the s1 excited state of para-methoxy-3-phenyl-3-methyl diazirine by ultrafast time resolved UV–Vis and IR spectroscopies and theory. J Am Chem Soc 131(38):13784
48. Bernardi F, Olivucci M, Robb MA, Vreven T, Soto J (2000) An ab initio study of the photochemical decomposition of 3,3-dimethyldiazirine. J Organ Chem 65(23):7847